Diverse Coordination Geometries Derived from Trisaminocyclohexane Ligands with Appended Outer-Sphere Hydrogen Bond Donors

Dr. Danushka M. Ekanayake, Patrick E. Sheridan, Dr. Sergey V. Lindeman, and Prof. Dr. Adam T. Fiedler*

Department of Chemistry, Marquette University, 1414 W. Clybourn St., Milwaukee, Wisconsin 53233, United States

Email contact: adam.fiedler@marquette.edu (A.T.F.)

Fax number: (+1) 414-288-7066

Abstract

With the aim of constructing hydrogen-bonding networks in synthetic complexes, two new ligands derived from *cis,cis*-1,3,5-triaminocyclohexane (TACH) have been prepared that feature pendant pyrrole or indole rings as outer-sphere H-bond donors. The TACH framework offers a facial arrangement of three *N*-donors, thereby mimicking common coordination motifs in the active sites of nonheme Fe and Cu enzymes. X-ray structural characterization of a series of Cu^{I}–X complexes (X = F, Cl, Br, NCS) revealed that these neutral ligands (H_3L^{R}, R = pyrrole or indole) coordinate in the intended facial N_3 manner, yielding four-coordinate complexes with idealized C_3 symmetry. The N-H units of the outer-sphere heterocycles form a hydrogen-bonding cavity around the axial (pseudo)halide ligand, as verified by crystallographic, spectroscopic, and computational analyses. Treatment of $H_3L^{pyrrole}$ and H_3L^{indole} with divalent transition metal chlorides ($M^{II}Cl_2$, M = Fe, Cu, Zn) causes one heterocycle to deprotonate and coordinate to the M(II) center, giving rise to tetradentate ligands with two remaining outer-sphere H-bond donors. Further ligand deprotonation is observed upon reaction with Ni(II) and Cu(II) salts with weakly-coordinating counteranions. The reported complexes highlight the versatility of TACH-based ligands with pendant H-bond donors, as the resulting scaffolds can support multiple protonation states, coordination geometries, and H-bonding interactions.

Introduction

It is well established that the remarkable catalytic activity of metalloenzymes is facilitated by a multitude of noncovalent interactions within each active site. A common feature is the presence of conserved outer-sphere (i.e., second-sphere) residues that hydrogen bond to first-sphere ligands and/or substrates coordinated to the metal ions(s).[1] These hydrogen bonding (H-bonding) interactions play a critical role in the recognition and activation of substrates, the stabilization of reactive catalytic intermediates, the tuning of redox potentials, proton transfer steps, and the prevention of deleterious side-reactions.[2] To account for the importance of second-sphere interactions in metalloenzyme catalysis, bio-inspired chemists have designed numerous polydentate ligands that feature outer-sphere groups capable of forming intramolecular H-bonds.[3] Early examples include "picket-fence" porphyrins with appended amide, urea, or carboxylic acid groups.[4] In nonheme systems, the vast majority of ligand scaffolds that support intramolecular H-bond networks have been based on tripodal, tetradentate motifs consisting of three arms attached to a central amine. Each ligand arm consists of metal-binding unit and an outer-sphere H-bond donor or acceptor. Following the pioneering work of Masuda, scaffolds derived from tris(2-pyridylmethyl)amine have been used to create H-bond interactions between first-sphere ligands and amido or amino groups attached to the pyridyl rings (Scheme 1a).[5] Similarly, the Borovik group has employed anionic tripodal ligands with one or more urea donors to stabilize M-O(H) units within a well-structured H-bond cavity (Scheme 1b).[6] Recent efforts to construct H-bonding networks have employed tripodal ligands with arms consisting of (hydroxy)pyridine,[7] quinoline,[8] sulfonamide,[9] phosphinic amide,[10] and pyrrole[11] donors.

A common structural motif in the active sites of nonheme iron, copper, and zinc enzymes is *facial* coordination by three histidine (His) residues[12] or the 2-His-1-carboxylate (aspartate or glutamate) triad.[13] It is widely recognized that such enzymes also utilize outer-sphere H-bond donors and acceptors to promote catalysis;[14] however, noncovalent interactions have generally been neglected in efforts to prepare synthetic models. For metalloenzymes with *fac*-triads, proper accounting of the primary and secondary coordination spheres requires the preparation of tridentate, facially-coordinating ligands that support H-bonding networks. To this end, Ward prepared tris(pyrazolyl)borate (Tp) scaffolds with H-bonding groups attached to the 3-position of the pyrazolyl ring (Scheme 1c).[15] Related Tp ligands were recently employed by the Warren group to incorporate H-bond acceptors into dicopper(II) complexes with bridging hydroxide and

diazene units.[16] The Fout[17] and Paine[18] groups have also prepared flexible dipodal ligands that place a pendant N-H groups in close proximity to an Fe(II) center (Scheme 1d). Yet despite these advances, facially-coordinating ligand scaffolds with second-sphere H-bond donors remain rare in the literature, especially when compared to the profusion of tetradentate, tripodal systems.

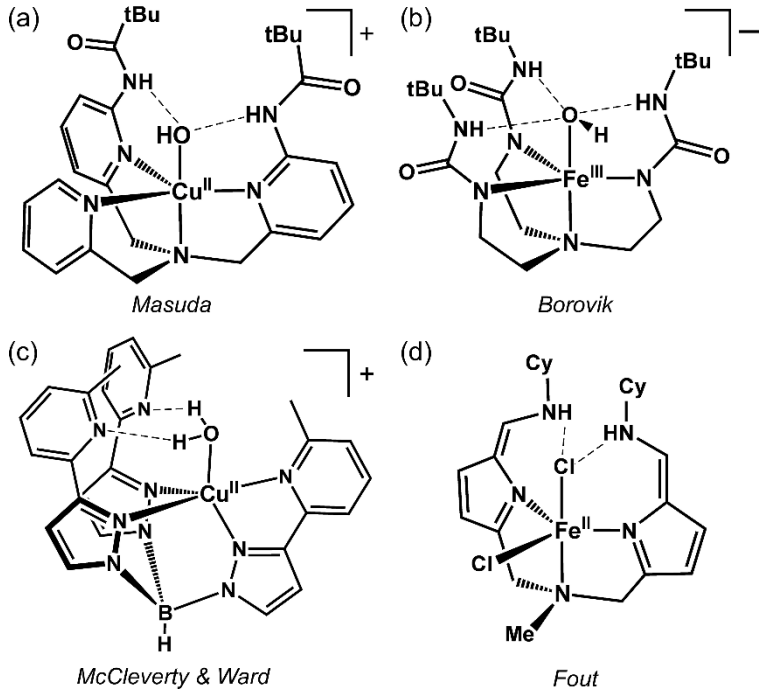

Scheme 1. Examples of multidentate ligands that support intramolecular H-bonding networks in transition metal complexes. *Top:* Tripodal scaffolds reported by (a) Masuda[5b] and (b) Borovik.[6e] *Bottom:* (c) a trispyrazolylborate ligand of Ward and McCleverty[15d] featuring outer-sphere pyridyl groups, and (d) dipodal, *fac*-coordinating ligand prepared by Fout.[17]

The *cis,cis*-1,3,5-triaminocyclohexane (TACH) scaffold provides a convenient template for neutral and constrained ligands with a facial arrangement of three *N*-donors. Although the $-NH_2$ groups occupy equatorial positions in free TACH, the ring adopts the axial conformation upon coordination due to the energetic benefit of forming three metal-nitrogen bonds (Scheme 2a). The amino groups are easily converted to imines via reaction with substituted aldehydes. Tridentate TACH-based ligands with imino donors have primarily been applied to copper chemistry,[19] although complexes with other first-row transition metals have been reported.[20] As described here, we have exploited this easily-modified platform to prepare facially-coordinating N_3 ligands with pyrrole ($H_3L^{pyrrole}$) or indole (H_3L^{indole}) units capable of serving as H-bond donors to first-sphere ligands (Scheme 2b). The coordination chemistry of these ligands with monovalent and

divalent metal ions has been examined via crystallographic and spectroscopic methods. The results indicate that $H_3L^{pyrrole}$ and H_3L^{indole} coordinate to Cu(I) ions in the intended manner to create rigid H-bonded cavities. The versatility of the ligands is evident in structures obtained with divalent metal ions of biological relevance (Zn, Cu, Ni, Fe), which display a fascinating variety of coordination geometries and intramolecular H-bonding networks.

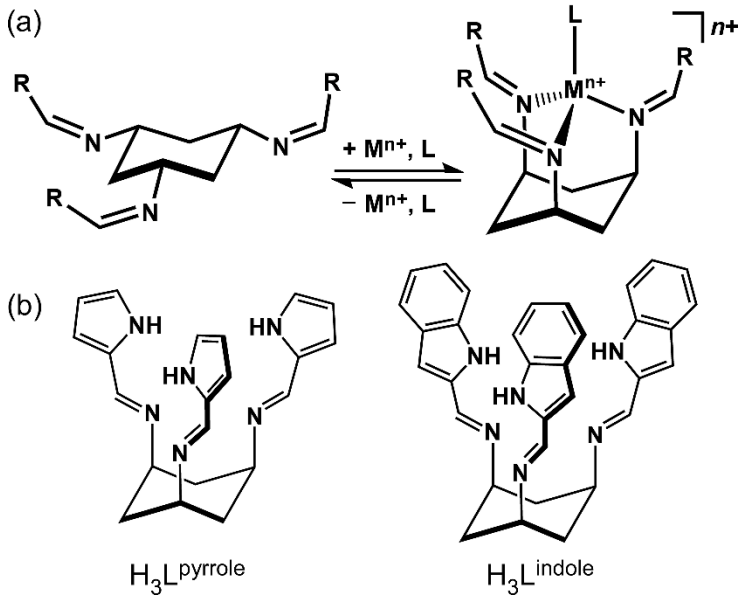

Scheme 2. (a) Coordination of TACH-based ligands; (b) structures of $H_3L^{pyrrole}$ and H_3L^{indole}.

Results and Discussion

Synthesis and X-ray Structures of Cu(I) Complexes. The $H_3L^{pyrrole}$ and H_3L^{indole} chelates were synthesized by condensation of neutralized TACH with three equivalents of the appropriate aldehyde in benzene. Water was removed by azeotropic distillation over 24 hours to provide the desired ligands, which were purified by recrystallization in CH_3CN (overall yields around 40% in both cases). Reaction of the TACH-based ligands with Cu^IX salts (X = Cl or Br) in THF yielded the yellow-colored complexes [CuCl($H_3L^{pyrrole}$)] (**1a**), [CuCl(H_3L^{indole})] (**1b**), [CuBr($H_3L^{pyrrole}$)] (**2a**), and [CuBr(H_3L^{indole})] (**2b**), where the "a" and "b" labels henceforth indicate complexes with ligands derived from $H_3L^{pyrrole}$ and H_3L^{indole}, respectively. The Cu(I) complexes are relatively stable in air, although slow decomposition is observed in aerobic solutions.

Yellow crystals suitable for X-ray crystallographic analysis were obtained by slow diffusion of Et_2O (or pentane) into concentrated CH_2Cl_2 solutions. Crystals of **1a** and **2a** are isomorphic in

the $P2_1/c$ space group, and each unit cell contains two symmetrically independent units with nearly identical geometries. Crystals of **1b** and **2b** are hexagonal in the $P6_1$ space group. Representative structures of **1a** and **2b** are shown in Figure 1(a,b). Selected metric parameters for copper(I)-chloride complexes (**1a** and **1b**) are summarized in Table 1, while those for the copper(I)-bromide complexes (**2a** and **2b**) are provided in the Supporting Information (Table S2). Each of the neutral Cu(I) complexes exhibit four-coordinate geometries comprised of a terminal halide and facially-capping $H_3L^{pyrrole}$ or H_3L^{indole} ligand. The TACH-based ligands confer nearly ideal three-fold rotational (C_3) symmetry along the Cu–X bond axis. The observed Cu–N bond distances fall within a narrow range of 2.07-2.10 Å, comparable to related Cu(I) complexes.[21] The average N–Cu–N bond angle is 97.6°, while the X–Cu–N bond angles are substantially larger with an average value of 119.7°. The coordination geometries of the Cu(I) complexes are best described as distorted trigonal pyramidal, consistent with the measured τ_4-values[22] of 0.83-0.86.

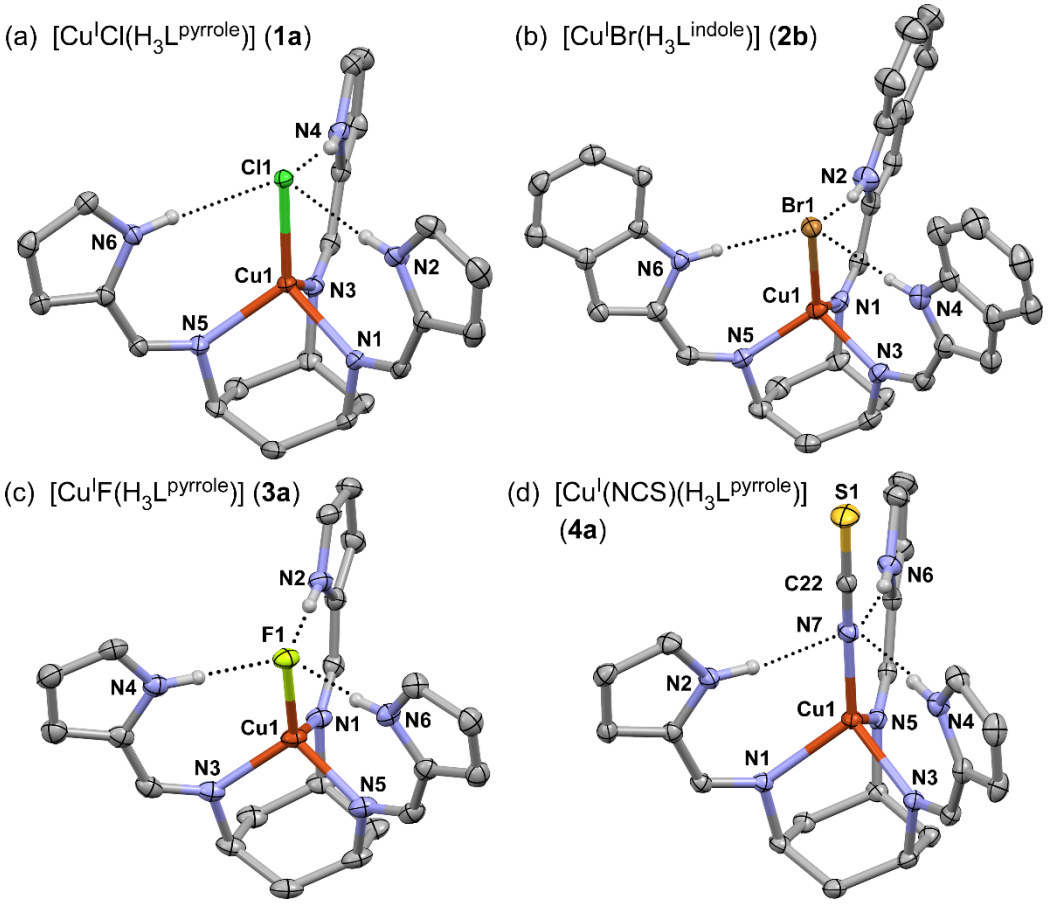

Figure 1. X-ray crystal structures of **1a**, **2b**, **3a**, and **4a** (50% probability ellipsoids). Only N–H hydrogens are shown for the sake of clarity. The dotted lines indicate the presence of H-bonds.

Table 1. Selected interatomic distances (Å), bond angles (°), and τ_4-parameters for TACH-based Copper(I)-Chloride and -Fluoride Complexes.

Parameter (X = Cl or F)	$[Cu^{I}Cl(H_3L^{pyrrole})]$ (**1a**) [a]	$[Cu^{I}Cl(H_3L^{indole})]$ (**1b**)	$[Cu^{I}Cl(L^{cinnamyl})]$ [b]	$[Cu^{I}F(H_3L^{pyrrole})]$ (**3a**)
Cu(1)–X(1)	2.3151(4)	2.3065(10)	2.285(3)	2.0684(8)
Cu(1)–N(1)	2.0766(14)	2.090(3)	2.08(1)	2.0155(13)
Cu(1)–N(3)	2.0961(15)	2.085(4)	2.086(9)	2.0038(13)
Cu(1)–N(5)	2.0713(14)	2.080(3)	2.076(9)	1.9988(13)
Cu–N (ave.)	*2.081*	*2.085*	*2.081*	*2.006*
N(2)···X(1)	3.1316(16)	3.086(3)	—	2.6858(16)
N(4)···X(1)	3.1412(16)	3.107(4)	—	2.6711(16)
N(6)···X(1)	3.1774(16)	3.134(3)	—	2.7037(15)
X(1)–Cu(1)–N(1)	119.74(4)	118.63(10)	122.8(3)	117.95(4)
X(1)–Cu(1)–N(3)	119.57(4)	117.96(9)	124.3(3)	117.00(5)
X(1)–Cu(1)–N(5)	119.59(4)	122.42(10)	120.6(3)	117.05(4)
X–Cu–N (ave.)	*119.6*	*119.7*	*122.6*	*117.3*
N(1)–Cu(1)–N(3)	96.48(6)	102.37(13)	91.4(4)	98.80(5)
N(1)–Cu(1)–N(5)	97.15(6)	95.93(12)	96.8(4)	99.01(5)
N(3)–Cu(1)–N(5)	99.32(6)	94.61(13)	93.1(4)	103.92(5)
N–Cu–N (ave.)	*97.7*	*97.6*	*93.8*	*100.6*
τ_4-value [c]	0.86	0.84	0.80	0.89

[a] Crystals of **1a** contain two symmetry-independent structures in each unit cell; values are only reported for one of the structures. [b] X-ray structure was reported in reference [19c] [c] The definition of the τ_4-parameter is provided in reference [22].

The solid-state structures reveal that, as intended, the axial halide ligand participates in H-bonding interactions with the three outer-sphere pyrrole/indole groups. The orientation adopted by the heterocyclic rings directs each N-H unit towards the cavity occupied by the halide ligand, resulting in N-H···X angles between 160 and 180°. The formation of H-bonds is evident from the average distances of 3.15 and 3.11 Å between the N-atoms of the heterocycles and the bound chloride atoms of **1a** and **1b**, respectively (Table 1). Previous studies have established that N···Cl distances of ~3.2 Å are characteristic of H-bonding interactions.[23] By comparison, the N···Br distances in **2a** and **2b** are longer by ~0.10 Å (Table S2), consistent with the increase in van der Waals radii from 1.75 Å (Cl) to 1.85 Å (Br).[24] The N···X distances in the H_3L^{indole}-based complexes (**1b**/**2b**) are shorter on average than those in the $H_3L^{pyrrole}$-based complexes (**1a**/**2a**),

suggesting that the more acidic indole group forms stronger H-bonds than pyrrole.[25] To gauge the structural impact of the H-bonding interactions, Tables 1 and S2 also include metric parameters for analogous Cu(I)–X complexes prepared by Walton and coworkers using a TACH-derived ligand ($L^{cinnamyl}$) that lacks outer-sphere H-bond donors.[19c] From this data, it is clear that the H-bonding networks in **1a/1b** and **2a/2b** cause a small but significant increase of 0.02-0.03 Å in Cu–X bond distances – a phenomenon observed in similar studies of metal-halide complexes with outer-sphere H-bond donors.[7c, 23b]

The reaction of $H_3L^{pyrrole}$ with $[Cu^I(CH_3CN)_4]PF_6$ in CH_2Cl_2 did not yield the intended cationic complex, $[Cu^I(CH_3CN)(H_3L^{pyrrole})]^+$. Instead, analysis of the resulting yellow crystals with X-ray crystallography revealed that the reaction generates the copper(I)-fluoride complex, $[Cu^IF(H_3L^{pyrrole})]$ (**3a**). Although the exact mechanism is not clear, the fluoride ligand clearly derives from the PF_6^- counteranion; indeed, there is ample precedent for the adventitious generation of fluoride ligands from the decomposition of PF_6^- or BF_4^-.[26] The overall structure of **3a** (Figure 1(c)) is analogous to those of **1a** and **2a** described above, including the presence of a rigid H-bonding cavity around the fluoride ligand. The average N···F distance of 2.69 Å (Table 1) is much shorter than the sum of the van der Waals radii (3.02 Å),[24] suggesting that the H-bonds in **3a** are considerably stronger than those of **1a** and **2a**. Examples of copper(I) complexes with terminal fluoride ligands are rare in the literature due to the intrinsic lability of the Cu(I)–F bond.[27] The majority of examples in the Cambridge Structural Database[28] are two-coordinate species consisting of a Cu(I)-F unit bound to a bulky heterocyclic carbene,[29] although three- and four-coordinate structures with bipyridine and phosphine ligands have also been reported.[30] The observed Cu(I)–F bond distance of 2.068 Å in **3a** (Table 1) is nearly identical to the value of 2.062 Å reported for $[Cu^IF(PPh_3)_3]$.[30a] The latter complex exhibits H-bonds between the fluoride ligand and an ethanolic solvate in the solid-state. Similarly, the Cu^I–F unit of **3a** is undoubtedly stabilized by the H-bonding cavity created by the $H_3L^{pyrrole}$ scaffold, which permits the isolation and crystallographic characterization of this unusual structure.

Finally, we prepared the complex $[Cu^I(NCS)(H_3L^{pyrrole})]$ (**4a**) to determine whether the H-bonding cavity could accommodate a triatomic pseudohalide ligand like thiocyanate. The resulting crystal structure, shown in Figure 1(d), reveals that the thiocyanate ligand coordinates to Cu(I) through its N atom. The thiocyanate coordination is nearly linear with an average Cu–N–C bond angle of 175.1° for the two independent structures in each unit cell. The N-H donors of the three

pyrrole rings are directed towards the bound N-atom, resulting in an average $N_{pyrrole}\cdots N_{NCS}$ distance of 2.96 Å. The impact of this H-bonding network on the vibrational modes of the NCS ligand is discussed below.

Synthesis and X-ray Structures of M(II) Complexes (M = Zn, Cu, Ni, Fe). With the goal of generating $[Fe^{II}Cl_2(H_3L)]$ complexes that could serve as models of nonheme iron(II) active-sites with facial 3-His coordination, the $H_3L^{pyrrole}$ and H_3L^{indole} scaffolds were each combined with one equivalent of $Fe^{II}Cl_2$ in THF to generate **5a** and **5b**, respectively. Reddish-orange crystals were obtained by slow diffusion of Et_2O in CH_2Cl_2, followed by analysis with X-ray crystallography. Instead of the target products, the resulting crystal structures revealed that one of the heterocyclic rings undergoes deprotonation, giving rise to an anionic pyrrolide (**5a**) or indolide (**5b**) donor that coordinates directly to Fe (Figure 2). Ligand deprotonation occurs in the absence of base, and chelation is paired with chloride loss to maintain the neutral charge of the resulting five-coordinate iron(II) complexes, $[Fe^{II}Cl(H_2L^{pyrrole})]$ (**5a**) and $[Fe^{II}Cl(H_2L^{indole})]$ (**5b**). The conversion of $H_3L^{pyrrole}$ and H_3L^{indole} into tetradentate and monoanionic ligands is favored by formation of a five-membered ring upon binding of the deprotonated heterocycle to the divalent Fe(II) ion, which is more Lewis acidic than monovalent Cu(I). At the same time, our computational results (*vide infra*) indicate that the observed structures are less sterically congested than the intended $[Fe^{II}Cl_2(H_3L)]$ complexes due to loss of a chloride ligand.

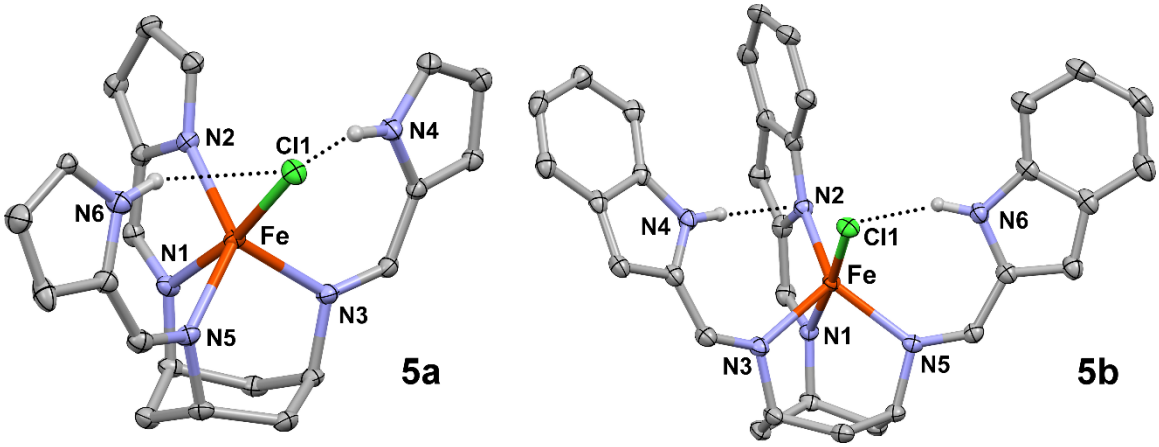

Figure 2. X-ray crystal structures of **5a** and **5b** (50% probability ellipsoids). Only N–H hydrogens are shown for the sake of clarity. The dotted lines indicate the presence of intramolecular H-bonds.

The structures of **5a** and **5b** exhibit distorted trigonal-bipyramidal geometries (τ_5 = 0.62 and 0.70, respectively)[31] in which the chloride ligand occupies one of the axial positions (see Table S3 for bond distances and angles). The two non-coordinating heterocycles each participate in H-bonding interactions with first-sphere ligands. In the case of **5a**, the N-H units of both outer-sphere pyrroles are directed towards the chloride ligand, and the observed N···Cl distances (3.195 ± 0.010 Å) are indicative of H-bonding in the solid state. As noted above for the Cu(I) complexes, the H-bonding interactions cause a lengthening the Fe–Cl bond, as the observed value of 2.419 Å in **5a** is considerably longer than bond distances reported for similar Fe^{II}–N_4Cl complexes (~2.31 Å) without H-bond networks.[32] Interestingly, the structure of **5b** reveals a different H-bonding arrangement. While one of the indole N-H groups is oriented towards the chloride with a N6···Cl1 distance of 3.202(1) Å, the other ring is rotated towards the anionic N-atom of the indolide donor (Figure 2). The N2···N4 distance of 3.142(1) Å and N4-H···N2 angle of 132° suggest that this second H-bond is rather weak – a conclusion supported by computational results presented below. The presence of only one H-bond involving the chloride ligand of **5b** results in an Fe–Cl bond distance of 2.372 Å (Table S3), which is shorter by 0.05 Å relative to **5a**.

The H_3L^{indole} chelate was also reacted with $CuCl_2$ and $ZnCl_2$ to assess its coordination chemistry with other divalent metal ions of biological relevance. X-ray crystal structures of the resulting complexes, [$Cu^{II}Cl(H_2L^{indole})$] (**6b**) and [$Zn^{II}Cl(H_2L^{indole})$] (**7b**), are shown in Figure S1, and metric parameters are summarized in Table S3. Both complexes are structurally analogous to **5b** with pentacoordinate geometries comprised of the tetradentate H_2L^{indole} anion and one chloride ligand. The geometry of the Cu^{II} complex (**6b**) is intermediate between the square-pyramidal and trigonal bipyramidal limits (τ_5 = 0.53), whereas the Zn^{II} complex (**7b**) is trigonal bipyramidal (τ_5 = 0.89). Like **5a**, the outer-sphere indole rings **6b** and **7b** are capable of H-bonding to either the chloride or indolide anions (Figure S1).

With the goal of generating TACH-based complexes with labile coordination sites, we also employed M(II) salts with weakly coordinating counteranions. Reaction of $H_3L^{pyrrole}$ with $Cu^{II}SO_4$ in CH_3OH generates a green-brown complex (**8a**) that was recrystallized from CH_2Cl_2/Et_2O. The resulting crystal structure revealed a neutral complex, [$Cu^{II}(HL^{pyrrole})$] (Figure 3), arising from pentadentate coordination of the dianionic $HL^{pyrrole}$ ligand. Deprotonation of the two pyrrole rings occurs spontaneously without added base, similar to formation of the H_2L^{indole}-based complexes above. Complex **8a** exhibits a distorted square-pyramidal (τ = 0.20) geometry in which the two

pyrrolide donors lie in the equatorial plane. The N5 donor deviates from the axial position due to constraints imposed by the TACH framework and the Cu–N5 bond distance is elongated to 2.375 Å. Reaction of $H_3L^{pyrrole}$ with $Ni^{II}(NO_3)_2$ in CH_3OH yields a reddish-orange complex (**9a**) that was characterized with X-ray crystallography. Like **8a**, the structure of **9a** consists of a dianionic $HL^{pyrrole}$ ligand with two pyrrolide donors. A key difference, however, is that the Ni(II) center adopts its preferred square-planar geometry, as the third arm of the TACH chelate remains unbound (the Ni···N5 distance is 2.7 Å). In both **8**a and **9a**, the one unprotonated pyrrole unit participates in a weak intramolecular H-bond with a pyrrolide donor (Figure 3).

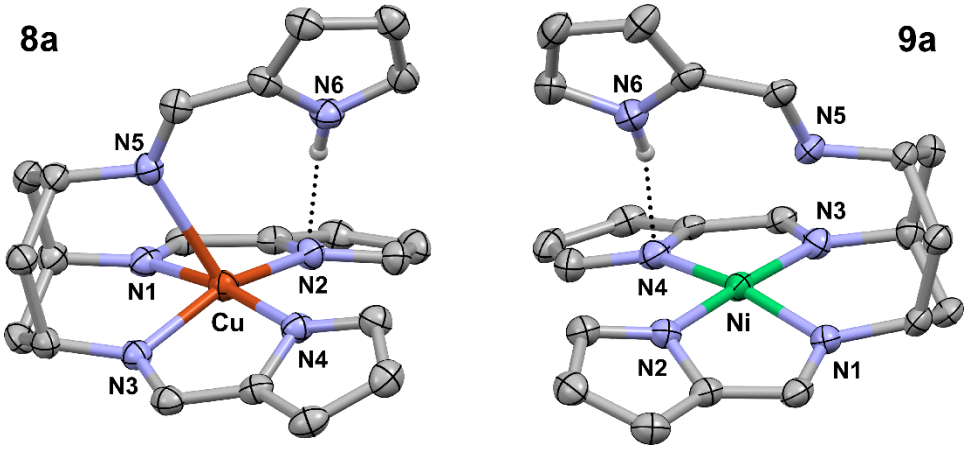

Figure 3. X-ray crystal structures of **8a** and **9a** (50% probability ellipsoids). Only N–H hydrogens are shown for the sake of clarity. The dotted lines indicate the presence of H-bonds. Selected bond lengths (Å) and angles (°) are provided in Table S4.

Spectroscopic Studies. (a) FT-IR Spectroscopy. The presence of H-bonding networks in the TACH-based complexes was further confirmed by FT-IR spectra of solid-state samples. The free ligands, $H_3L^{pyrrole}$ and H_3L^{indole}, exhibit N–H stretching modes at ν(N-H) = 3338 and 3443 cm^{-1}, respectively, in addition to an intense peak near 1630 cm^{-1} arising from the N=C stretch of the imine group. The less sterically hindered $H_3L^{pyrrole}$ ligand likely forms intermolecular H-bonds between N–H and –N=C units in the solid state, resulting in a lower ν(N-H) frequency than the H_3L^{indole} ligand. FTIR spectra of **1a** measured in the solid state and CH_2Cl_2 solution exhibit similar ν(N-H) and ν(N=C) frequencies (Figure S2), indicating that the molecular structure and H-bonding network of the X-ray structure are maintained in solution. Table 2 provides experimental and computed ν(N-H) frequencies for the TACH-based ligands and copper(I) complexes, and FTIR

spectra of the $H_3L^{pyrrole}$ series are shown in Figure 4. In most cases, three ν(N-H) peaks are observed for the Cu(I) complexes: the weaker, higher-energy feature arises from the symmetric combination of N-H stretching motions, whereas the two intense features at lower energy are assigned to the pair of nearly-degenerate asymmetric combinations (Figure 4). The ν(N-H) frequencies of Cu(I) complexes are shifted to lower energy relative to the free ligands as a result of intramolecular H-bonds, which facilitate electron donation from the anionic X ligand into the σ* orbital of the N-H bond. The magnitude of the bathochromic shift, Δν(N-H), reflects the strength of the H-bonding interaction. Across the series, Δν(N-H) shifts follow the order F >> Cl > Br > NCS (Table 2) – consistent with relative H-bond strengths inferred from the X-ray structural data (*vide supra*). In the case of **4a**, the ν(N=C) mode of the NCS ligand is observed at 2023 cm^{-1}, consistent with *N*-based thiocyanate coordination.[33] The ν(N=C) frequency of **4a** is downshifted by 67 cm^{-1} relative to the value measured for the related complex, $[Cu^{I}(NCS)(L^{mesityl})]$, that lacks H-bond interactions (Figure S3; $L^{mesityl}$ is a TACH-derived ligand with pendant mesityl rings instead of *N*-heterocycles[19a]).

FTIR data for the divalent metal complexes are summarized in Table S5. Complexes with the formula $[M^{II}Cl(H_2L^{indole})]$ (M = Fe (**5b**), Cu (**6b**), and Zn (**7b**)) each exhibit two ν(N-H) peaks with downshifts of ~250 cm^{-1} relative to free H_3L^{indole}. Whereas only one ν(N=C) peak appears in spectra of the C_3-symmetric Cu(I) complexes, the less symmetric M^{II}–Cl complexes generally exhibit three peaks at slightly lower frequencies. Finally, spectra of $[Cu^{II}(HL^{pyrrole})]$ (**8a**) and $[Ni^{II}(HL^{pyrrole})]$ (**9a**) each display one ν(N-H) feature at 3301 and 3355 cm^{-1}, respectively. The Δν(N-H) shifts for these complexes are quite small (< 40 cm^{-1}), confirming the weakness of the intramolecular H-bond formed between the pyrrole and pyrrolide units.

Table 2. N-H Stretching Frequencies (Experimental and DFT-Computed) and H-bond Enthalpies for TACH-based Ligands and Copper(I) Complexes.

Compound	Exper. frequencies (cm^{-1}) [a]		DFT frequencies (cm^{-1}) [b]		ΔH per H-bond (kcal/mol) [d]
	ν(N–H)	Δν(N–H), ave.[c]	ν(N–H) , ave.	Δν(N–H), ave.[c]	
$H_3L^{pyrrole}$	3338		3500, 3493, 3492		
[CuF($H_3L^{pyrrole}$)] (**3a**)	3102, 3028	–273	3140, 3056, 3034	–418	–6.6
[CuCl($H_3L^{pyrrole}$)] (**1a**)	3252, 3208, 3195	–120	3260, 3224, 3217	–261	–4.8
[CuBr($H_3L^{pyrrole}$)] (**2a**)	3266, 3222, 3207	–106	3277, 3249, 3240	–240	–4.5
[Cu(NCS)($H_3L^{pyrrole}$)] (**4a**)	3282 (*br*)	–56	3345, 3326, 3313	–167	–3.4
H_3L^{indole}	3443		3492, 3484, 3482		
[CuCl(H_3L^{indole})] (**1b**)	3244, 3211, 3179	–232	3276, 3244, 3231	–236	–4.3
[CuBr(H_3L^{indole})] (**2b**)	3285, 3241, 3223	–193	3297, 3267, 3251	–214	–4.1

[a] Experimental FTIR spectra were measured using solid-state samples. [b] The computed ν(N-H) frequencies were scaled by the factor of 96% reported by Merrick *et al.* for the B3LYP functional.[34] [c] Δν(N–H) is the average shift in ν(N-H) frequencies between the complex and free ligand ($H_3L^{pyrrole}$ or H_3L^{indole}). [d] The ΔH-values are derived from the average of the computed and scaled $\Delta\nu_{(N-H)}$ frequency shifts using the methodology reported by Iogansen and Belkova.[35] The values reflect the enthalpic contribution of a single H-bond.

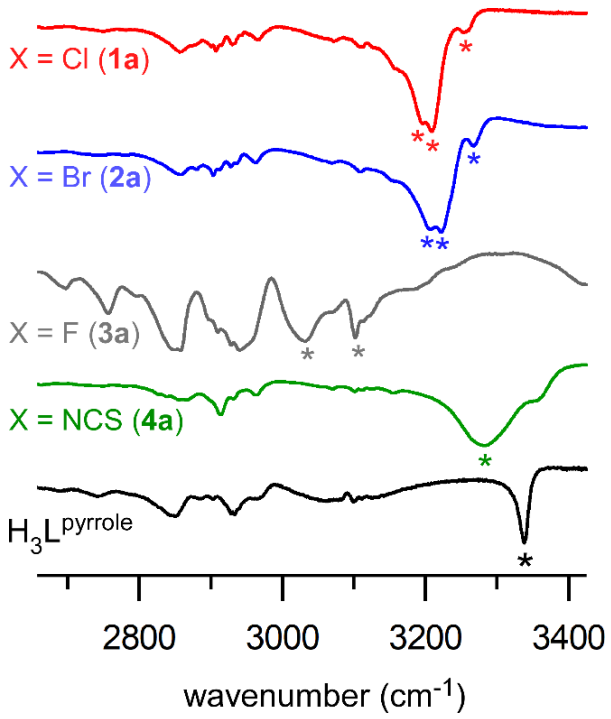

Figure 4. Solid-state FTIR spectra of $H_3L^{pyrrole}$ and [CuX($H_3L^{pyrrole}$)]; X = Cl (**1a**), Br (**2a**), F (**3a**), NCS (**4a**). Peaks arising from ν(N-H) modes are indicated with an asterisk (*).

(b) ^1H NMR Spectroscopy. The NH resonances of the free ligands appear as broad peaks at δ_{NH} = 9.6 and 9.1 ppm in the ^{1}H NMR spectra of $H_3L^{pyrrole}$ and H_3L^{indole}, respectively. As evident in Figure 5, the NH peak shifts downfield and becomes dramatically sharper in spectra of the $H_3L^{pyrrole}$-based Cu(I) complexes in $CDCl_3$ or CD_2Cl_2. The sharpness of the N-H resonances is further confirmation that intramolecular N-H···X interactions persist in solution, and the sizable downfield shifts ($\Delta\delta_{NH} = \delta_{NH,complex} - \delta_{NH,ligand}$) reflect deshielding of the NH donor as a result of H-bond formation. Within each series, the magnitude of $\Delta\delta_{NH}$ is proportional to the H-bond strength, and the observed trend of F (3.9) >> Cl (2.8) > Br (2.6) > NCS (1.9) is consistent with the FTIR data. Indeed, a plot of $\Delta\delta_{NH}$ versus the electronegativity of the X-ligand reveals a linear relationship, as shown in Figure S4. The NH resonance of the cooper(I)-fluoride complex (**3a**), which exhibits the largest $\Delta\delta_{NH}$ shift, appears as a doublet due coupling with the ^{19}F nucleus (J_{H-F} = 37 Hz in $CDCl_3$; Figure 5). The ^{19}F splitting is larger (J_{H-F} = 46 MHz) and better resolved in CD_2Cl_2 (Figure S5). Slightly larger $\Delta\delta_{NH}$ shifts are observed for the H_3L^{indole}-based Cu(I) complexes (**1b** and **2b**; Figure S6), supporting the hypothesis that indole is a stronger H-bond donor than pyrrole.

^{1}H NMR spectra of the Cu(II) and Fe(II) complexes yield less insight into outer-sphere interactions because the δ_{NH}-values are affected by the paramagnetic ions. Spectra of the diamagnetic Zn^{II} (**7b**) and low-spin Ni^{II} (**9a**) complexes revealed relatively small $\Delta\delta_{NH}$ shifts of 1.7 and 1.6 ppm, respectively (Figure S7). Only one NH resonance is observed for **7b**, suggesting that the outer-sphere indole units are equivalent in solution.

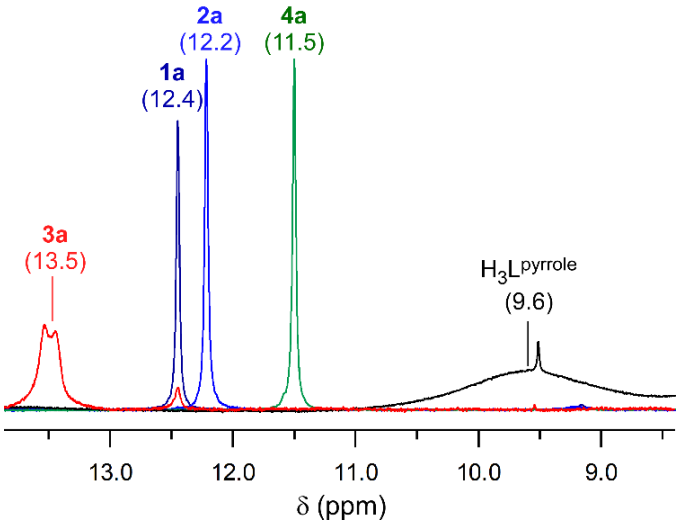

Figure 5. Downfield region of the ^{1}H NMR spectra of $H_3L^{pyrrole}$ and [CuX($H_3L^{pyrrole}$)]; X = Cl (**1a**), Br (**2a**), F (**3a**), NCS (**4a**). Data were measured at room temperature in $CDCl_3$ for all samples. The peaks arise from NH resonances and chemical shifts (δ_{NH}) are indicated in parentheses.

Computational Studies. The energetic contributions of the intramolecular H-bonds were quantified using density functional theory (DFT) calculations. Geometry-optimized models derived from B3LYP calculations display good overall agreement with the X-ray data, although DFT tends to overestimate the M–X/N bond lengths by ~0.05 Å (Table S6). Computed ν(N-H) frequencies for the Cu(I) complexes were scaled according to the factor reported by Merrick *et al*.[34] (Table 2). The predicted frequencies are remarkably close to the experimental values, indicating that DFT provides an accurate description of the H-bonding interactions. One exception is the discrepancy between experimental and computed ν(N-H) frequencies of the $H_3L^{pyrrole}$ ligand; however, as noted above, the lower experimental value likely reflects the presence of intermolecular H-bonds in the solid-state, whereas the DFT value corresponds to a gas-phase molecule. Most importantly, the computed ν(N-H) frequencies nicely reproduce the observed trends across the [$Cu^{I}X(H_3L^{pyrrole})$] and [$Cu^{I}X(H_3L^{indole})$] series (Table 2).

The H-bond formation enthalpies, ΔH_{HB}, can be estimated from the computed downshifts of ν(N-H) frequencies, as demonstrated in previous studies by Iogansen and Belkova.[35] Applying this methodology to the Cu(I) series provides ΔH_{HB} values (per H-bond) that range from –6.6 kcal/mol for **3a** (X = F) to –3.4 kcal/mol for **4a** (X = NCS). These values are consistent with H-bond formation enthalpies reported for related complexes with N-H···X-M units.[36] Because the Cu(I) complexes contain three equivalent H-bonds, the computed ΔH_{HB} values suggest that the

entire H-bonding network provides a net stabilization of ~10-20 kcal/mol. Table S7 summarizes DFT ν(N-H) frequencies and H-bond formation enthalpies for the divalent complexes. The computed ΔH_{HB} values of the Cu(II)-Cl complex (**6b**) are lower than those of its Cu(I)-Cl analogs (**1a** and **1b**), indicating that the greater Lewis acidity of the Cu(II) ion weakens the H-bonding interaction by pulling electron density away from the chloride ligand. The DFT results also suggest that H-bonds between outer-sphere heterocycles and bound pyrrolide/indolide donors, as observed in some X-ray structures, are substantially weaker than those involving (pseudo)halide ligands. This conclusion is consistent the small Δν(N-H) shifts measured experimentally for **8a** and **9a** (Table S5).

DFT calculations were also used to rationalize the tendency of the TACH-based ligands to undergo deprotonation upon complexation with divalent ions. Geometry optimizations of hypothetical $[M^{II}Cl_2(H_3L^{pyrrole})]$ species (M = Fe or Zn) led to dissociation of one imine donor from the $H_3L^{pyrrole}$ chelate, giving rise to four-coordinate $[M^{II}Cl_2(\kappa^2\text{-}H_3L^{pyrrole})]$ structures (see Figure S8). The pyrrole of the dissociated arm maintains a H-bonding interaction with the proximal Cl ligand. From the calculations, it is clear that the cavity created by κ^3-coordination of the neutral $H_3L^{pyrrole}$/H_3L^{indole} ligands can only accommodate one (pseudo)halide ligand. Although formation of a hypothetical $[M^{II}X(H_3L)]^+$ complex would relieve steric strain, our results suggest that such species undergo facile ligand deprotonation due to favorable coordination of the resulting pyrrolide/indolide donor to the M(II) ion.

Conclusion

This report has described the synthesis and coordination chemistry of two TACH-based ligands ($H_3L^{pyrrole}$ and H_3L^{indole}) that possess pendant pyrrole and indole groups capable of serving as second-sphere H-bond donors. In contrast to the vast library of tripodal and tetradentate ligands that support intramolecular H-bonding networks, $H_3L^{pyrrole}$ and H_3L^{indole} were intended to coordinate in a tridentate and facial manner, thereby mimicking 3-His and 2-His-1-carboxylate motifs found in numerous metalloenzymes. The ligands bind to Cu^IX salts (X = Cl, Br, NCS) in the intended fashion, yielding four-coordinate complexes that feature three H-bonding interactions between the (pseudo)halide ligand and N-H donors of the pyrrole/indole rings (Figure 1). Reaction of $H_3L^{pyrrole}$ with $[Cu^I(CH_3CN)_4]PF_6$ triggered decomposition of the PF_6^- counteranion, yielding the unique copper(I)-fluoride complex **3a**. The often unstable Cu(I)–F bond is stabilized by the

H-bonding cavity created by the outer-sphere pyrrole rings. The presence of H-bonding interactions in the solid-state was verified by X-ray crystallography and FTIR spectroscopic studies of each of the six Cu(I) complexes reported here. The NH resonances in ^{1}H NMR spectra of the TACH-based ligands exhibit dramatic downfield shifts upon metal coordination, indicating that the H-bond networks are also present in solution samples. As expected, the strength of the H-bonds is dependent on the electronegativity of the axial X-ligand, following the order F >> Cl > Br > NCS. Analysis of ν(N-H) frequencies computed by DFT suggest that the H-bond formation enthalpies (ΔH_{HB}) range from 3-7 kcal/mol (Table 2), meaning that the H-bonding cavities of the Cu(I) complexes lead to a net stabilization of ~10-20 kcal/mol.

Reaction of $H_3L^{pyrrole}$ and H_3L^{indole} with divalent M(II) cations (M = Fe, Ni, Cu, Zn) results in spontaneous deprotonation and coordination of one or two of the heterocyclic rings. The process is energetically favored by binding of the resulting pyrrolide/indolide donor(s) to generate stable five-membered chelate rings. The heterocyclic units that remain in the outer sphere establish H-bonds with anionic first-sphere ligands, although these interactions are generally weaker than those observed for the Cu(I) analogs. DFT calculations suggest that the coordination geometries of the $[M^{II}Cl(H_2L^{pyrrole/indole})]$ complexes (**5a**, **5b**, **6b**, and 7**b)** relieve the steric strain of the intended $[M^{II}X_2(H_3L)]$ species. Further deprotonation is observed when $H_3L^{pyrrole}$ is reacted with M(II) salts with weakly-coordinating counteranions, giving rise to the dianionic $HL^{pyrrole}$ ligand in **8a** and **9a**. Collectively, these results demonstrate that the $H_3L^{pyrrole}$ and H_3L^{indole} scaffolds can exist in various charged states and adopt multiple denticities. This remarkable versatility is evident in the different coordination geometries displayed by the M(II) complexes, such as trigonal-bipyramidal, square pyramidal, and square planar.

Finally, this study has also highlighted some of the limitations of using $H_3L^{pyrrole}$ and H_3L^{indole} to model the active sites of metalloenzymes. The well-structured H-bonding cavity created by the three outer-sphere heterocycles can only accommodate one ligand, and thus coordination of additional ligands or substrates requires dissociation of one of the TACH arms. The stabilization afforded by multiple H-bonds also appears to limit the reactivity of the complexes towards small molecules, like O_2. Another drawback is the tendency of the pyrrole and indole groups to undergo deprotonation and coordination to Lewis acidic ions. Future modeling efforts will be directed towards the preparation of asymmetric TACH-based chelates that are less sterically hindered and provide greater access to the metal ion. These second-generation ligands will also employ outer-

sphere moieties that are more resistant to deprotonation, thereby avoiding direct coordination of the H-bond donors. Thus, the insights presented here will guide the development of future TACH-based ligands that accurately replicate the *fac* coordination geometry and second-sphere interactions of numerous nonheme metalloenzymes.

Experimental and Computational Procedures

Materials and Physical Methods: Unless otherwise noted, solvents and reagents were purchased from commercial sources and used without further purification. Solvents were dried over CaH_2 or NaH prior to distillation under Argon gas. Several freeze-pump-thaw cycles were performed to remove oxygen and other gases, and the solvents were stored inside the glovebox over activated molecular sieves. All complexes were synthesized and handled under an inert atmosphere using a Vacuum Atmospheres Omni-Lab glovebox. The ligand precursor *cis,cis*-1,3,5-triaminocyclohexane·3HBr (TACH·3HBr) was prepared according to a previously reported procedure.[37] Elemental analysis data was collected at Midwest Microlab, LLC, in Indianapolis, IN. Infrared spectra were measured using a Nicolet iS50 FTIR spectrometer with attenuated total reflectance capabilities for solid-state samples. The baselines of some IR spectra were digitally adjusted using the software program Spectragryph. ^{1}H NMR spectra were collected at room temperature using Varian 400 MHz or 600 MHz spectrometers, and standard baselines corrections were applied. NMR spectra of the ligands and transition metal complexes are provided in Figures S5 and S9-S17.

Synthesis of $H_3L^{pyrrole}$. *cis,cis*-1,3,5-Triaminocyclohexane·3HBr (1.03 g, 2.77 mmol) was added to a 250 mL round bottom flask and dissolved in an aqueous solution of NaOH (5 mL, 0.33 g, 8.3 mmol), followed by addition of benzene (100 mL).[38] The flask was equipped with a Dean-Stark trap and the mixture heated in a fume hood until nearly all of the water was removed. Afterwards, a solution of pyrrole-2-carboxaldehyde (0.797 g, 8.38 mmol) in benzene was added to the flask. The resulting mixture was heated to reflux for 24 hr., during which time the water byproduct was eliminated through azeotropic distillation. The resulting orange-brown solution was cooled to room temperature, followed by addition of water (25 mL). The aqueous phase was extracted with $CHCl_3$ (3 x 50 mL), and the combined organic extracts were dried over $MgSO_4$ and filtered. Evaporation of solvent provided the crude product. Recrystallization using hot anhydrous CH_3CN provided $H_3L^{pyrrole}$ as a light brown solid, which was used without further purification. Yield = 37%. Elemental analysis calcd (%) for $C_{21}H_{24}N_6 \cdot H_2O$ (M_W = 378.5 g mol^{-1}): C, 66.64; H,

6.92; N, 22.21. Found: C, 66.86; H, 6.36; N, 21.15. Yield = 0.45 g (45%). FTIR (solid): ν = 3338 (ν_{N-H}), 2933, 2849, 1633 ($\nu_{N=C}$) cm^{-1}. ^1H NMR (600 MHz, $CDCl_3$): δ = 9.6 (br, N-*H*), 8.08 (*s*, 3H, C*H*=N), 6.78 (*s*, 3H, *H*-pyrrole), 6.45 (*s*, 3H, *H*-pyrrole), 6.18 (*s*, 3H, *H*-pyrrole), 3.39 (*br*, 3H, –C*H*–N=), 2.00-1.75 (*m*, 6H, –CH_2–) ppm.

Synthesis of H_3L^{indole}. The H_3L^{indole} ligand was prepared according to the same procedure as $H_3L^{pyrrole}$. TACH·3HBr (1.03 g, 2.77 mmol) was deprotonated in aqueous solution using NaOH (0.33 g, 8.3 mmol). Benzene (100 mL) was added and the mixture refluxed in a fume hood using a Dean-Stark apparatus to remove water.[38] After addition of indole-2-carboxaldehyde (1.20 g, 8.27 mmol), a Dean-Stark distillation under reflux was performed for 24 hr. The mixture was cooled to room temperature and water (25 mL) was added. The product was extracted with $CHCl_3$ (3 x 50 mL), dried over $MgSO_4$, and filtered. Removal of solvent provided the crude product, which was washed with Et_2O to remove aldehyde starting material. Recrystallization using CH_3CN provided H_3L^{indole} as a brown solid. Yield = 45%. Elemental analysis calcd (%) for $C_{33}H_{30}N_6 \cdot H_2O$ (M_W = 528.6 g mol^{-1}): C, 74.98; H, 6.10; N, 15.90. Found: C, 75.19; H, 5.81; N, 15.61. FTIR (solid): ν = 3443 (ν_{N-H}), 3051, 2927, 2855, 1629 ($\nu_{N=C}$), 1613 cm^{-1}. ^1H NMR (400 MHz, $CDCl_3$): δ = 9.10 (*br*, 3H, -N*H*), 8.32 (s, 3H, C*H*=N), 7.62 (*d*, 3H, *H*-indole), 7.36 (*d*, 3H, *H*-indole), 7.24 (3H, *H*-indole, obscured by solvent peak), 7.09 (*t*, 3H, *H*-indole), 6.78 (*s*, 3H, *H*-indole), 3.58 (*m*, 3H, –C*H*–N=), 1.96 (*m*, 6H, –CH_2–) ppm.

[$Cu^ICl(H_3L^{pyrrole})$] (1a). Copper(I) chloride (41.0 mg, 0.414 mmol) was added to a solution of $H_3L^{pyrrole}$ (149 mg, 0.414 mmol) in THF. The resulting bright yellow solution was stirred for 2 hr. and then filtered through a pad of Celite. The solvent was removed under vacuum to obtain the yellow product. Yield = 124 mg (65%). Slow diffusion of pentane into a concentrated CH_2Cl_2 solution provided yellow crystals of **1a** suitable for X-ray crystallography. Elemental analysis calcd (%) for $C_{21}H_{24}ClCuN_6$ (M_W = 459.5 g mol^{-1}): C, 54.90; H, 5.27; N, 18.29. Found: C, 55.32; H, 5.68; N, 18.48. FTIR (solid): ν = 3252 (ν_{N-H}), 3208 (ν_{N-H}), 3195 (ν_{N-H}), 2906, 2856, 1618 ($\nu_{N=C}$) cm^{-1}. ^1H NMR (400 MHz, $CDCl_3$): δ = 12.4 (*s*, 3H, N–*H*), 7.87 (*s*, 3H, C*H*=N), 7.10 (*s*, 3H, *H*-pyrrole), 6.56 (*s*, 3H, *H*-pyrrole), 6.18 (*s*, 3H, *H*-pyrrole), 3.85 (*br*, 3H, –C*H*–N=), 2.21 (*d*, 3H, –C*H*H–), 2.04 (*d*, 3H, –CH*H*–) ppm.

[$Cu^ICl(H_3L^{indole})$] (1b). Copper(I) chloride (20.0 mg, 0.20 mmol) was added to a solution of H_3L^{indole} (100 mg, 0.196 mmol) in THF. The resulting yellow solution was stirred for 2 hr. and

filtered through a plug of Celite. Removal of solvent under vacuum provided the product as yellow flakes. The crude material was recrystallized by diffusion of pentane into a CH_2Cl_2 solution. Yield = 66 mg (55%). Elemental analysis calcd (%) for $C_{33}H_{30}ClCuN_6$ (M_W = 609.6 g mol^{-1}): C, 65.02; H, 4.96; N, 13.79. Found: C, 64.49; H, 5.29; N, 13.36. FTIR (solid): ν = 3244 (ν_{N-H}), 3211 (ν_{N-H}), 3179 (ν_{N-H}), 2865, 1608 ($\nu_{N=C}$) cm^{-1}. ^{1}H NMR (400 MHz, $CDCl_3$): δ = 12.6 (*s*, 3H, N–*H*), 8.16 (*s*, 3H, C*H*=N), 7.76 (*d*, 3H, *H*-indole), 7.55 (*d*, 3H, *H*-indole), 7.30 (*t*, 3H, *H*-indole), 7.04 (*t*, 3H, *H*-indole), 6.86 (*s*, 3H, *H*-indole), 4.03 (*s*, 3H, –C*H*–N=), 2.35 (*d*, 3H, –CH*H*–), 2.17 (*d*, 3H, –C*H*H–) ppm.

[Cu^{I}Br(H$_3$L^{pyrrole})] (2a). This complex was prepared according to the same procedure as **1a**, with the exception that CuBr was used instead of CuCl. Yellow crystals for diffraction analysis were obtained by vapor diffusion of Et_2O into a concentrated solution of **2a** in CH_2Cl_2. Yield = 70%. Elemental analysis calcd (%) for $C_{21}H_{24}BrCuN_6$ (M_W = 503.9 g mol^{-1}): C, 50.05; H, 4.80; N, 16.68. Found: C, 49.85; H, 4.81; N, 16.45. FTIR (solid): ν = 3266 (ν_{N-H}), 3222 (ν_{N-H}), 3207 (ν_{N-H}), 2960, 2903, 2856, 1615 ($\nu_{N=C}$) cm^{-1}. ^{1}H NMR (600 MHz, $CDCl_3$): δ = 12.2 (*s*, 3H, N–*H*), 7.90 (*s*, 3H, C*H*=N), 7.10 (*s*, 3H, *H*-pyrrole), 6.55 (*s*, 3H, *H*-pyrrole), 6.18 (*s*, 3H, *H*-pyrrole), 3.86 (*br*, 3H, –C*H*–N=), 2.23 (*d*, 3H, –C*H*H–), 2.06 (*d*, 3H, –CH*H*–) ppm.

[Cu^{I}Br(H$_3$L^{indole})] (2b). This complex was prepared according to the same procedure as **1b**, with the exception that CuBr was used instead of CuCl. Vapor diffusion of Et_2O into a concentrated solution of **2b** in CH_2Cl_2 provided yellow needles suitable for crystallographic studies. Yield = 65%. Elemental analysis calcd (%) for $C_{33}H_{30}BrCuN_6$ (M_W = 654.1 g mol^{-1}): C, 60.60; H, 4.62; N, 12.85. Found: C, 59.83; H, 4.75; N, 12.48. FTIR (solid): ν = 3285 (ν_{N-H}), 3241 (ν_{N-H}), 3223 (ν_{N-H}), 2913, 2870, 1609 ($\nu_{N=C}$) cm^{-1}. ^{1}H NMR (600 MHz, $CDCl_3$): δ = 12.3 (*s*, 3H, N–*H*), 8.17 (*s*, 3H, C*H*=N), 7.76 (*d*, 3H, *H*-indole), 7.56 (*d*, 3H, *H*-indole), 7.29 (*t*, 3H, *H*-indole), 7.05 (*t*, 3H, *H*-indole), 6.85 (*s*, 3H, *H*-indole), 4.03 (*s*, 3H, –C*H*–N=), 2.36 (*d*, 3H, –CH*H*–), 2.19 (*d*, 3H, –C*H*H–) ppm.

[Cu^{I}F(H$_3$L^{pyrrole})] (3a). [Cu^{I}(CH$_3$CN)$_4$]PF$_6$ (103 mg, 0.276 mmol) was added to a solution of H$_3$L^{pyrrole} (98 mg, 0.27 mmol) in CH_2Cl_2. The solution was stirred for one hour and filtered through a Celite pad. The filtrate was concentrated and layered with hexane, yielding flat yellow crystals of **3a** suitable for X-ray diffraction studies. Yield = 34% Elemental analysis calcd (%) for $C_{21}H_{24}CuFN_6$ (M_W = 443.0 g mol^{-1}): C, 56.94; H, 5.46; N, 18.97. Found: C, 56.82; H, 5.43; N,

17.31. We were not able to obtain analytically pure samples of **3a**, perhaps because the complex arises from the decomposition of starting material. FTIR (solid): ν = 3102 (ν_{N-H}), 3028 (ν_{N-H}), 2937, 2846, 1617 ($\nu_{N=C}$) cm^{-1}. ^1H NMR (600 MHz, $CDCl_3$): δ = 13.5 (*d*, J_{HF} = 37 Hz, 3H, N–*H*), 7.83 (*s*, 3H, C*H*=N), 7.21 (*s*, 3H, *H*-pyrrole), 6.56 (*s*, 3H, *H*-pyrrole), 6.20 (*s*, 3H, *H*-pyrrole), 3.94 (*s*, 3H, –C*H*–N=), 2.23 (*d*, 3H, –C*H*H–), 2.01 (*d*, 3H, –CH*H*–) ppm.

[Cu^{I}(NCS)($H_3L^{pyrrole}$)] (4a). A suspension of CuSCN (31.2 mg, 0.256 mmol) in CH_3CN was added to a solution of $H_3L^{pyrrole}$ (91 mg, 0.25 mmol) in a mixture of THF and CH_3CN. The slightly turbid solution was stirred for two hours and then filtered. Removal of the solvent under vacuum provided orange crystalline material that was used without further purification. Yield = 86 mg (70 %). Elemental analysis calcd (%) for $C_{22}H_{24}CuN_7S$ (M_W = 482.1 g mol^{-1}): C, 54.81; H, 5.02; N, 20.34. Found: C, 54.42; H, 5.09; N, 19.83. FTIR (solid): ν = 3282 (*br*, ν_{N-H}), 2913, 2016 ($\nu_{N=CS}$), 1614 ($\nu_{N=C}$) cm^{-1}. ^1H NMR (600 MHz, $CDCl_3$): δ = 11.5 (*s*, 3H, N–*H*), 7.88 (*s*, 3H, C*H*=N), 7.30 (*s*, 3H, *H*-pyrrole), 6.58 (*s*, 3H, *H*-pyrrole), 6.23 (*s*, 3H, *H*-pyrrole), 3.83 (*s*, 3H, –C*H*–N=), 2.20 (*d*, 3H, –C*H*H–), 1.98 (*d*, 3H, –CH*H*–) ppm.

[$Fe^{II}Cl(H_2L^{pyrrole})$] (5a). $FeCl_2$ (44 mg, 0.35 mmol) and $H_3L^{pyrrole}$ (125 mg, 0.347 mmol) and were combined in THF (10 mL) and stirred overnight. The turbid orange mixture was filtered and concentrated under vacuum. Addition of Et_2O resulted in precipitation of the crude product. After decanting the solvent, the resulting solid was dried and washed multiple times with Et_2O to remove impurities. Vapor diffusion of Et_2O into a THF solution of **5a** over the course of two days produced small orange crystals suitable for X-ray crystallography. Yield = 156 mg (65%). Elemental analysis calcd (%) for $C_{21}H_{23}ClFeN_6$ (M_W = 450.7 g mol^{-1}): C, 55.96; H, 5.14, N, 18.64. Found: C, 55.44; H, 5.33; N, 17.75. FTIR (solid): ν = 3223 (ν_{N-H}), 2928, 1623 ($\nu_{N=C}$), 1609 ($\nu_{N=C}$), 1595 ($\nu_{N=C}$) cm^{-1}. ^1H NMR (400 MHz, CD_3CN): δ = 333 (1H), 306 (1H), 262 (2H), 167 (2H), 90 (1H), 66 (1H), 55 (1H), 27 (1H), 10.1 (*br*, 2H), 5.0 (2H), –0.6 (2H), –10.9 (2H), –14.2 (2H), –16.4 (2H), –55 (1 H) ppm.

[$Fe^{II}Cl(H_2L^{indole})$] (5b). $FeCl_2$ (25 mg, 0.20 mmol) and H_3L^{indole} (102 mg, 0.200 mmol) were mixed in THF (10 mL) and the resulting bright orange solution was stirred overnight. The solution was filtered and the solvent removed under vacuum. The crude product was dissolved in a minimal amount of CH_2Cl_2 and layered with Et_2O to obtain orangish-red crystals suitable for crystallographic analysis. Yield = 72 mg (60%). Elemental analysis calcd (%) for

$C_{33}H_{29}ClFeN_6 \cdot 0.5CH_2Cl_2$ (M_W = 600.9 g mol^{-1}): C, 62.54; H, 4.70; N, 13.06. Found: C, 62.87; H, 4.83; N, 13.10. FTIR (solid): ν = 3206 (ν_{N-H}), 3182 (ν_{N-H}), 3050, 2918, 2857, 1613 ($\nu_{N=C}$), 1603 ($\nu_{N=C}$) cm^{-1}.

[Cu^{II}Cl(H$_2$L^{indole})] (6b). Anhydrous $CuCl_2$ (26 mg, 0.19 mmol) was added to a stirring solution of H_3L^{indole} (100 mg, 0.196 mmol) in CH_3OH, resulting in formation of a brown-colored precipitate. The reaction mixture was stirred for 30 min. and the solid product was isolated by filtration. Yield = 60 mg (52%). Dark brown crystals suitable for X-ray diffraction experiments were obtained by diffusion of Et_2O into a concentrated CH_2Cl_2 solution. Elemental analysis calcd (%) for $C_{33}H_{29}ClCuN_6$ (M_W = 608.6 g mol^{-1}): C, 65.12; H, 4.80; N, 13.81. Found: C, 64.97; H, 5.05; N, 13.42. FTIR (solid): ν = 3215 (ν_{N-H}), 3185 (ν_{N-H}), 3057, 2917, 2868, 1623 ($\nu_{N=C}$), 1610 ($\nu_{N=C}$), 1596 ($\nu_{N=C}$) cm^{-1}.

[Zn^{II}Cl(H$_2$L^{indole})] (7b). Anhydrous $ZnCl_2$ (26 g, 0.19 mmol) was added to a solution of H_3L^{indole} (0.097 g, 0.19 mmol) in THF, and the reaction mixture was stirred for 2 hr. The solution was then filtered through a pad of Celite. The solvent was removed under vacuum to yield an oily brown product, which was dissolved in CH_2Cl_2 and filtered again through Celite. Removal of solvent provided the crude product; trace impurities were removed by washing with Et_2O. Yield = 67 mg (58 %). Colorless rectangular crystals suitable for X-ray crystallography were generated by slow evaporation of CH_2Cl_2 solvent under vacuum. Elemental analysis calcd (%) for $C_{33}H_{29}N_6ZnCl$ (M_W = 610.5 g mol^{-1}): C, 64.93; H, 4.79; N, 13.77. Found: C, 64.24; H, 4.74; N, 13.55. FTIR (solid): ν = 3200 (ν_{N-H}), 3180 (ν_{N-H}), 2959, 2920, 2851, 1636 ($\nu_{N=C}$), 1625 ($\nu_{N=C}$), 1612 ($\nu_{N=C}$) cm^{-1}. ^{1}H NMR (600 MHz, CD_2Cl_2): δ = 11.0 (*s*, 2H, N–*H*), 8.94 (*d*, 1H, *H*-indolide), 8.25 (*s*, 2H, C*H*=N), 8.13 (*s*, 1H, C*H*=N), 7.62 (*d*, 1H, *H*-indolide), 7.52 (*t*, 2H, *H*-indolide), 7.50 (*d*, 1H, *H*-indole), 7.11 (*m*, 3H, *H*-indolide), 6.99 (*t*, 2H, *H*-indole), 6.98 (*s*, 2H, *H*-indole), 6.79 (*s*, 2H, *H*-indolide), 6.78 (*s*, 1H, *H*-indole), 4.20 (3H, –C*H*–N=), 2.86 (*d*, 1H, –CH*H*–), 2.55 (*d*, 1H, –C*H*H–), 2.44 (*d*, 2H, –CH*H*–), 2.01 (*d*, 2H, –C*H*H–).

[Cu^{II}(HL^{pyrrole})] (8a). The $H_3L^{pyrrole}$ ligand (0.100 g, 0.277 mmol) and $CuSO_4 \cdot 5H_2O$ (69.0 mg, 0.276 mmol) were combined in CH_3OH. The mixture was stirred for 30 min., during which time an olive-green precipitate was formed. The precipitate was collected via filtration and washed with cold CH_3OH. The crude material was purified by vapor diffusion of Et_2O into a concentrated CH_2Cl_2 solution, giving rise to dark-brown crystals suitable for crystallographic studies. Yield =

64 mg (55%). Elemental analysis calcd (%) for $C_{21}H_{22}CuN_6$ (M_W = 422.0 g mol^{-1}): C, 59.77; H, 5.25; N, 19.92. Found: C, 59.89; H, 5.62; N, 19.84. FTIR (solid): ν = 3301 (ν_{N-H}), 2864, 1627 ($\nu_{N=C}$), 1605 ($\nu_{N=C}$), 1585 ($\nu_{N=C}$) cm^{-1}.

[Ni^{II}(HL^{pyrrole})] (9a). The $H_3L^{pyrrole}$ ligand (92 mg, 0.26 mmol) and $Ni(NO_3)_2 \cdot 6H_2O$ (81 mg, 0.28 mmol) were combined in CH_3OH, causing immediate formation of a red-orange precipitate. The mixture was stirred for an hour and the solution was decanted from the precipitate. The solid was dissolved in CH_2Cl_2, filtered through Celite, and the solvent removed to yield the desired product. Yield = 21 mg (19%) Red-orange crystals suitable for X-ray crystallography were generated by slow evaporation of CH_2Cl_2 solvent. Elemental analysis calcd (%) for $C_{21}H_{22}N_6Ni$ (M_W = 417.1 g mol^{-1}): C, 60.47; H, 5.32; N, 20.15. Found: C, 58.10; H, 5.30; N, 20.18. FTIR (solid): ν = 3355 (ν_{N-H}), 3081, 1635 ($\nu_{N=C}$), 1587 ($\nu_{N=C}$) cm^{-1}. ^{1}H NMR (400 MHz, CD_2Cl_2,): δ = 11.2 (*br*, 1H, N–*H*), 8.85 (*s*, 1H, C*H*=N), 7.85 (*s*, 2H, C*H*=N), 7.16 (*s*, 2H, *H*-pyrrole), 6.70 (*s*, 1H, *H*-pyrrole), 6.59 (*s*, 2H, *H*-pyrrole), 6.46 (*s*, 1H, *H*-pyrrole), 6.27 (*s*, 2H, *H*-pyrrole), 6.11 (*s*, 1H, *H*-pyrrole), 4.11 (*s*, 1H, –C*H*–N=), 3.99 (*s*, 2H, –C*H*–N=), 2.12 (*m*, 3H, –CH_2–), 1.99 (*d*, 1H, –CH*H*–), 1.72 (*d*, 2H, –C*H*H–) ppm.

X-ray Crystallography. Crystals of the TACH-based complexes were grown via procedures described above. X-ray-diffraction intensities of the resulting single crystals were measured at 100 K with an Oxford Diffraction SuperNova kappa-diffractometer (Rigaku Corp.) consisting of dual Cu/Mo X-ray sources, X-ray mirror optics, an Atlas CCD detector, and a low-temperature Cryojet device (Oxford Instruments). Data was processed using the CrysAlisPro program package, and numerical absorption correction based on Gaussian integration over a multifaceted crystal model was applied. This procedure was followed by empirical absorption correction involving spherical harmonics from the SCALE3 ABSPACK scaling algorithm. Structures were solved within the Olex2 crystallographic package[39] and refined using the program SHELXL.[40] Non-hydrogen atoms were refined using anisotropic displacement parameters. Hydrogen atoms were generally positioned geometrically and refined using appropriate restraints for bond lengths and angles, while the torsion angles of methyl hydrogens were optimized to fit residual electron density. The solvent-mask procedure was applied to structures of **1b** and **2b**. Crystals of **8a** are pseudo-monoclinic, quasi-merohedral regular twins (180° rotation around *y**). Similarly, twinning (4:1) was observed for crystals of **9a** with 150° rotation around the *y*-axis. Enantiomers of complex **7b** crystallize separately in the chiral space group of $P2_12_12_1$. Further information regarding data

collection, analysis, and crystallographic parameters are summarized in Table S1 for each complex.

Density Functional Theory (DFT) Calculations. ORCA software package (version 4.0) developed by Dr. F. Neese (MPI-KoFo)[41] was used to perform DFT calculations of the free ligands ($H_3L^{pyrrole}$ and H_3L^{indole}) and select transition metal complexes. All calculations employed Becke's three-parameter hybrid functional for exchange and the Lee-Yang-Parr correlation functional (B3LYP),[42] in combination with the Karlsruhe valence triple-ζ basis set with polarization functions (def2-TZVP).[43] Computational efficiency was improved by applying the resolution of identity and chain of sphere (RIJCOSX) approximations[44] with the appropriate auxiliary basis sets.[45] X-ray crystallographic structures served as the starting points of geometry optimizations, and convergence to local energy minima was verified by the lack of imaginary modes in the numerical frequency calculation. Computed frequencies were scaled by factors reported by Moran and Radom for DFT functionals.[34] Following a previously-reported approach,[35] enthalpies for hydrogen bond formation ($\Delta H_{H\text{-bond}}$) were estimated using the equation: $\Delta H_{H\text{-bond}}$ (kcal/mol) = $-18|\Delta\nu|/(|\Delta\nu| + 720)$, where $\Delta\nu$ is the computed downshift in N–H frequencies upon formation of intramolecular H-bonds.

Acknowledgements

The authors are grateful for financial support from U.S. National Science Foundation (CHE-1900562 to A.T.F.). DFT calculations were performed on the Raj Cluster at Marquette University, which was built with funds from the National Science Foundation (CNS-1828649). The authors thank Alexander J. Pienkos for assistance in ligand preparation.

Keywords

Coordination Modes, Hydrogen bonds, Ligand design, Structure Elucidation, Tridentate Ligands

Data Availability Statement

Additional data that support the findings of this study are available in the supplementary material of this article. Deposition numbers 2279023-2279034 contain the supplementary crystallographic data for this paper. These data are provided free of charge by the joint Cambridge Crystallographic Data Centre (https://www.ccdc.cam.ac.uk/structures).

References

[1] (a) S.-O. Shan, D. Herschlag, *Methods Enzymol.* **1999**, *308*, 246-276; (b) S. P. de Visser, *Chem. - Eur. J.* **2020**, *26*, 5308-5327.

[2] (a) S. A. Martinis, W. M. Atkins, P. S. Stayton, S. G. Sligar, *J. Am. Chem. Soc.* **1989**, *111*, 9252; (b) D. B. Goodin, D. E. McRee, *Biochemistry* **1993**, *32*, 3313; (c) B. A. Springer, S. G. Sligar, J. S. Olson, G. N. Phillips, Jr., *Chem. Rev.* **1994**, *94*, 699-714; (d) R. A. Edwards, M. M. Whittaker, J. W. Whittaker, E. N. Baker, G. B. Jameson, *Biochemistry* **2001**, *40*, 15-27; (e) C. K. Vance, A.-F. Miller, *Biochemistry* **2001**, *40*, 13079-13087; (f) J. Xie, E. Yikilmaz, A.-F. Miller, T. C. Brunold, *J. Am. Chem. Soc.* **2002**, *124*, 3769-3774; (g) D. R. Tomchick, P. Phan, M. Cymborowski, W. Minor, T. R. Holman, *Biochemistry* **2001**, *40*, 7509-7517; (h) S. T. Stripp, B. R. Duffus, V. Fourmond, C. Leger, S. Leimkuehler, S. Hirota, Y. Hu, A. Jasniewski, H. Ogata, M. W. Ribbe, *Chem. Rev.* **2022**, *122*, 11900-11973.

[3] (a) S. A. Cook, E. A. Hill, A. S. Borovik, *Biochemistry* **2015**, *54*, 4167-4180; (b) M. W. Drover, *Chem. Soc. Rev.* **2022**, *51*, 1861-1880; (c) M. Zhao, H.-B. Wang, L.-N. Ji, Z.-W. Mao, *Chem. Soc. Rev.* **2013**, *42*, 8360-8375; (d) L. V. A. Hale, N. K. Szymczak, *ACS Catal.* **2018**, *8*, 6446-6461.

[4] (a) J. P. Collman, R. R. Gagne, C. Reed, T. R. Halbert, G. Lang, W. T. Robinson, *J. Am. Chem. Soc.* **1975**, *97*, 1427; (b) M. Momenteau, C. A. Reed, *Chem. Rev.* **1994**, *94*, 659; (c) G. E. Wuenschell, C. Tetreau, D. Lavalette, C. A. Reed, *J. Am. Chem. Soc.* **1992**, *114*, 3346-3355; (d) C. Y. Yeh, C. J. Chang, D. G. Nocera, *J. Am. Chem. Soc.* **2001**, *123*, 1513-1514.

[5] (a) M. Harata, K. Jitsukawa, H. Masuda, H. Einaga, *Chem. Lett.* **1995**, 61-62; (b) M. Harata, K. Jitsukawa, H. Masuda, H. Einaga, *Bull. Chem. Soc. Jpn.* **1998**, *71*, 637-645; (c) A. Wada, M. Harata, K. Hasegawa, K. Jitsukawa, H. Masuda, M. Mukai, T. Kitagawa, H. Einaga, *Angew. Chem. Int. Ed.* **1998**, *37*, 798-799; (d) S. Ogo, R. Yamahara, M. Roach, T. Suenobu, M. Aki, T. Ogura, T. Kitagawa, H. Masuda, S. Fukuzumi, Y. Watanabe, *Inorg. Chem.* **2002**, *41*, 5513-5520; (e) S. Yamaguchi, A. Wada, Y. Funahashi, S. Nagatomo, T. Kitagawa, K. Jitsukawa, H. Masuda, *Eur. J. Inorg. Chem.* **2003**, 4378-4386; (f) J. Matsumoto, T. Suzuki, Y. Kajita, H. Masuda, *Dalton Trans.* **2012**, *41*, 4107-4117; (g) V. Yadav, J. B. Gordon, M. A. Siegler, D. P. Goldberg, *J. Am. Chem. Soc.* **2019**, *141*, 10148-10153.

[6] (a) A. S. Borovik, *Acc. Chem. Res.* **2005**, *38*, 54-61; (b) R. L. Shook, A. S. Borovik, *Inorg. Chem.* **2010**, *49*, 3646-3660; (c) S. A. Cook, A. S. Borovik, *Acc. Chem. Res.* **2015**, *48*, 2407-2414; (d) J. L. Lee, D. L. Ross, S. K. Barman, J. W. Ziller, A. S. Borovik, *Inorg. Chem.* **2021**, *60*, 13759-13783; (e) C. E. MacBeth, R. Gupta, K. R. Mitchell-Koch, V. G. Young, G. H. Lushington, W. H. Thompson, M. P. Hendrich, A. S. Borovik, *J. Am. Chem. Soc.* **2004**, *126*, 2556-2567.

[7] (a) E. W. Dahl, J. J. Kiernicki, M. Zeller, N. K. Szymczak, *J. Am. Chem. Soc.* **2018**, *140*, 10075-10079; (b) E. W. Dahl, H. T. Dong, N. K. Szymczak, *Chem. Commun.* **2018**, *54*, 892-895; (c) C. M. Moore, N. K. Szymczak, *Chem. Commun.* **2015**, *51*, 5490-5492.

[8] C. M. Moore, N. K. Szymczak, *Dalton Trans.* **2012**, *41*, 7886-7889.

[9] J. R. Jones, J. W. Ziller, A. S. Borovik, *Inorg. Chem.* **2017**, *56*, 1112-1120.

[10] V. F. Oswald, A. C. Weitz, S. Biswas, J. W. Ziller, M. P. Hendrich, A. S. Borovik, *Inorg. Chem.* **2018**, *57*, 13341-13350.

[11] (a) E. M. Matson, J. A. Bertke, A. R. Fout, *Inorg. Chem.* **2014**, *53*, 4450-4458; (b) Y. J. Park, M. N. Penas-Defrutos, M. J. Drummond, Z. Gordon, O. R. Kelly, I. J. Garvey, K. L. Gullett, M. Garcia-Melchor, A. R. Fout, *Inorg. Chem.* **2022**, *61*, 8182-8192.

[12] (a) A. R. Diebold, M. L. Neidig, G. R. Moran, G. D. Straganz, E. I. Solomon, *Biochemistry* **2010**, *49*, 6945-6952; (b) J. W. Godden, S. Turley, D. C. Teller, E. T. Adman, M. Y. Liu, W. J. Payne, J. LeGall, *Science* **1991**, *253*, 438; (c) D. W. Christianson, C. A. Fierke, *Acc. Chem. Res.* **1996**, *29*, 331-339.

[13] K. D. Koehntop, J. P. Emerson, L. Que, *J. Biol. Inorg. Chem.* **2005**, *10*, 87-93.

[14] (a) A. J. Mitchell, N. P. Dunham, R. J. Martinie, J. A. Bergman, C. J. Pollock, K. Hu, B. D. Allen, W.-c. Chang, A. Silakov, J. M. Bollinger, C. Krebs, A. K. Boal, *J. Am. Chem. Soc.* **2017**, *139*, 13830-13836; (b) L. L. Kiefer, S. A. Paterno, C. A. Fierke, *J. Am. Chem. Soc.* **1995**, *117*, 6831; (c) A. C. Merkle, N. Lehnert, *Dalton Trans.* **2012**, *41*, 3355-3368.

[15] (a) B. S. Hammes, X. Luo, M. W. Carrano, C. J. Carrano, *Inorg. Chim. Acta* **2002**, *341*, 33-38; (b) D. A. Bardwell, J. C. Jeffery, P. L. Jones, J. A. McCleverty, M. D. Ward, *J. Chem. Soc., Dalton Trans.* **1995**, 2921; (c) B. S. Hammes, X. Luo, B. S. Chohan, M. W. Carrano, C. J. Carrano, *J. Chem. Soc., Dalton Trans.* **2002**, 3374-3380; (d) E. R. Humphrey, K. L. V. Mann, Z. R. Reeves, A. Behrendt, J. C. Jeffery, J. P. Maher, J. A. McCleverty, M. D. Ward, *New J. Chem.* **1999**, *23*, 417-424; (e) P. L. Jones, J. C. Jeffery, J. P. Maher, J. A. McCleverty, P. H. Rieger, M. D. Ward, *Inorg. Chem.* **1997**, *36*, 3088-3095.

[16] (a) E. J. Gardner, C. R. Cobb, J. A. Bertke, T. H. Warren, *Inorg. Chem.* **2019**, *58*, 11248-11255; (b) E. J. Gardner, S. C. Marguet, C. R. Cobb, D. M. Pham, J. A. M. Beringer, J. A. Bertke, H. S. Shafaat, T. H. Warren, *J. Am. Chem. Soc.* **2021**, *143*, 15960-15974.

[17] E. M. Matson, Z. Gordon, B. Lin, M. J. Nilges, A. R. Fout, *Dalton Trans.* **2014**, *43*, 16992-16995.

[18] (a) S. Chatterjee, T. K. Paine, *Inorg. Chem.* **2015**, *54*, 1720-1727; (b) S. Chatterjee, D. Sheet, T. K. Paine, *Chem. Commun.* **2013**, *49*, 10251-10253.

[19] (a) M. Cushion, P. Ebrahimpour, M. F. Haddow, A. J. Hallett, S. M. Mansell, A. G. Orpen, D. F. Wass, *Dalton Trans.* **2009**, 1632-1635; (b) I. Shimizu, Y. Morimoto, D. Faltermeier, M. Kerscher, S. Paria, T. Abe, H. Sugimoto, N. Fujieda, K. Asano, T. Suzuki, P. Comba, S. Itoh, *Inorg. Chem.* **2017**, *56*, 9634-9645; (c) A. K. Nairn, S. J. Archibald, R. Bhalla, C. J. Boxwell, A. C. Whitwood, P. H. Walton, *Dalton Trans.* **2006**, 1790-1795; (d) P. Ebrahimpour, M. Cushion, M. F. Haddow, A. J. Hallett, D. F. Wass, *Dalton Trans.* **2010**, *39*, 10910-10919; (e) P. Ebrahimpour, M. F. Haddow, D. F. Wass, *Inorg. Chem.* **2013**, *52*, 3765-3771; (f) C. J. Boxwell, R. Bhalla, L. Cronin, S. S. Turner, P. H. Walton, *J. Chem. Soc., Dalton Trans.* **1998**, 2449-2450; (g) B. Greener, L. Cronin, G. D. Wilson, P. H.

Walton, *J. Chem. Soc., Dalton Trans.* **1996**, 401; (h) Y. Lan, Y. Morimoto, I. Shimizu, H. Sugimoto, S. Itoh, *Inorg. Chem.*

[20] (a) S. S. Rocks, W. W. Brennessel, T. E. Machonkin, P. L. Holland, *Inorg. Chem.* **2010**, *49*, 10914-10929; (b) L. Cronin, S. P. Foxon, P. J. Lusby, P. H. Walton, *JBIC, J. Biol. Inorg. Chem.* **2001**, *6*, 367-377; (c) B. Greener, S. P. Foxon, P. H. Walton, *New J. Chem.* **2000**, *24*, 269-273; (d) S. J. Archibald, S. P. Foxon, J. D. Freeman, J. E. Hobson, R. N. Perutz, P. H. Walton, *J. Chem. Soc., Dalton Trans.* **2002**, 2797-2799; (e) L. Cronin, B. Greener, S. P. Foxon, S. L. Heath, P. H. Walton, *Inorg. Chem.* **1997**, *36*, 2594-2600; (f) L. Cronin, P. H. Walton, *Chem. Commun.* **2003**, 1572-1573; (g) B. Greener, M. H. Moore, P. H. Walton, *Chem. Commun.* **1996**, 27.

[21] (a) Y. Zhao, X. Wang, R. Kaneyama, K. Kodama, T. Hirose, *ChemistrySelect* **2020**, *5*, 4152-4159; (b) I. Kinoshita, A. Hamazawa, T. Nishioka, H. Adachi, H. Suzuki, Y. Miyazaki, A. Tsuboyama, S. Okada, M. Hoshino, *Chem. Phys. Lett.* **2003**, *371*, 451-457; (c) P. Liebhaeuser, K. Keisers, A. Hoffmann, T. Schnappinger, I. Sommer, A. Thoma, C. Wilfer, R. Schoch, K. Stuehrenberg, M. Bauer, M. Duerr, I. Ivanovic-Burmazovic, S. Herres-Pawlis, *Chem. - Eur. J.* **2017**, *23*, 12171-12183.

[22] L. Yang, D. R. Powell, R. P. Houser, *Dalton Trans.* **2007**, 955-964.

[23] (a) J. Emsley, *Chem. Soc. Rev.* **1980**, *9*, 91-124; (b) N. S. Sickerman, Y. J. Park, G. K. Y. Ng, J. E. Bates, M. Hilkert, J. W. Ziller, F. Furche, A. S. Borovik, *Dalton Trans.* **2012**, *41*, 4358-4364.

[24] A. Bondi, *J. Phys. Chem.* **1964**, *68*, 441.

[25] F. G. Bordwell, G. E. Drucker, H. E. Fried, *J. Org. Chem.* **1981**, *46*, 632.

[26] (a) J. Olguin, S. Bernes, L. Gasque, *Crystals* **2012**, *2*, 1357-1365; (b) R. R. Jacobson, Z. Tyeklar, K. D. Karlin, J. Zubieta, *Inorg. Chem.* **1991**, *30*, 2035; (c) M. Schatz, M. Becker, F. Thaler, F. Hampel, S. Schindler, R. R. Jacobson, Z. Tyeklar, N. N. Murthy, P. Ghosh, Q. Chen, J. Zubieta, K. D. Karlin, *Inorg. Chem.* **2001**, *40*, 2312-2322; (d) J. Ackermann, F. Meyer, H. Pritzkow, *Inorg. Chim. Acta* **2004**, *357*, 3703-3711; (e) J. Reedijk, *Comments Inorg. Chem.* **1982**, *1*, 379.

[27] K. Fagnou, M. Lautens, *Angew. Chem. Int. Ed.* **2002**, *41*, 26-47.

[28] Cambridge crystallographic database search (CSD version 5.42, updated February 2021)

[29] (a) T. Fujihara, T. Xu, K. Semba, J. Terao, Y. Tsuji, *Angew. Chem., Int. Ed.* **2011**, *50*, 523; (b) J. W. Hall, F. Seeberger, M. F. Mahon, M. K. Whittlesey, *Organometallics* **2020**, *39*, 227-233; (c) T. Vergote, F. Nahra, A. Welle, M. Luhmer, J. Wouters, N. Mager, O. Riant, T. Leyssens, *Chem. - Eur. J.* **2012**, *18*, 793; (d) L. Kuehn, A. F. Eichhorn, D. Schmidt, T. B. Marder, U. Radius, *J. Organomet. Chem.* **2020**, *919*, 121249; (e) L. S. Sharninghausen, A. F. Brooks, W. P. Winton, K. J. Makaravage, P. J. H. Scott, M. S. Sanford, *J. Am. Chem. Soc.* **2020**, *142*, 7362-7367.

[30] (a) D. J. Gulliver, W. Levason, M. Webster, *Inorg. Chim. Acta* **1981**, *52*, 153; (b) C. Rasson, O. Riant, *Org. Process Res. Dev.* **2020**, *24*, 835-840; (c) Y. Liu, C. Chen, H. Li, K.-W. Huang, J. Tan, Z. Weng, *Organometallics* **2013**, *32*, 6587-6592.

[31] A. W. Addison, T. N. Rao, J. Reedijk, J. Vanrijn, G. C. Verschoor, *J. Chem. Soc., Dalton Trans.* **1984**, 1349-1356.

[32] M. Kim, Y.-U. Kim, J. Han, *Polyhedron* **2007**, *26*, 4003-4008.

[33] K. Nakamoto, *Infrared and Raman Spectra of Inorganic and Coordination Compounds*, 5th ed., John Wiley & Sons, Inc., New York, **1997**.

[34] J. P. Merrick, D. Moran, L. Radom, *J. Phys. Chem. A* **2007**, *111*, 11683-11700.

[35] (a) N. V. Belkova, L. M. Epstein, O. A. Filippov, E. S. Shubina, *Spectrosc. Prop. Inorg. Organomet. Compd.* **2012**, *43*, 1-28; (b) N. V. Kireev, O. A. Filippov, A. A. Pavlov, L. M. Epstein, V. D. Makhaev, V. P. Dyadchenko, E. S. Shubina, N. V. Belkova, *Inorg. Chem.* **2018**, *57*, 1656-1664; (c) A. V. Iogansen, G. A. Kurkchi, V. M. Furman, V. P. Glazunov, S. E. Odinokov, *Zh. Prikl. Spektrosk.* **1980**, *33*, 460.

[36] J. C. M. Rivas, S. L. Hinchley, L. Metteau, S. Parsons, *Dalton Trans.* **2006**, 2316-2322.

[37] M. de Loos, J. H. van Esch, R. M. Kellogg, B. L. Feringa, *Tetrahedron* **2007**, *63*, 7285-7301.

[38] Although our procedure used benzene as solvent, related TACH-based ligands have also been generated using toluene. For examples, see references 19a, 19d, and 19e.

[39] O. V. Dolomanov, L. J. Bourhis, R. J. Gildea, J. A. K. Howard, H. Puschmann, *J. Appl. Crystallogr.* **2009**, *42*, 339-341.

[40] (a) G. M. Sheldrick, *Acta Crystallogr. Sect. A* **2008**, *64*, 112-122; (b) G. M. Sheldrick, *Acta Crystallogr., Sect. C: Struct. Chem.* **2015**, *71*, 3-8.

[41] (a) F. Neese; (b) F. Neese, *Wiley Interdisciplinary Reviews: Computational Molecular Science* **2012**, *2*, 73-78.

[42] (a) A. D. Becke, *J. Chem. Phys.* **1993**, *98*, 5648-5652; (b) C. T. Lee, W. T. Yang, R. G. Parr, *Physical Review B* **1988**, *37*, 785-789.

[43] F. Weigend, R. Ahlrichs, *Phys. Chem. Chem. Phys.* **2005**, *7*, 3297-3305.

[44] F. Neese, F. Wennmohs, A. Hansen, U. Becker, *Chem. Phys.* **2009**, *356*, 98-109.

[45] F. Weigend, *Phys. Chem. Chem. Phys.* **2006**, *8*, 1057-1065.

Table of Contents

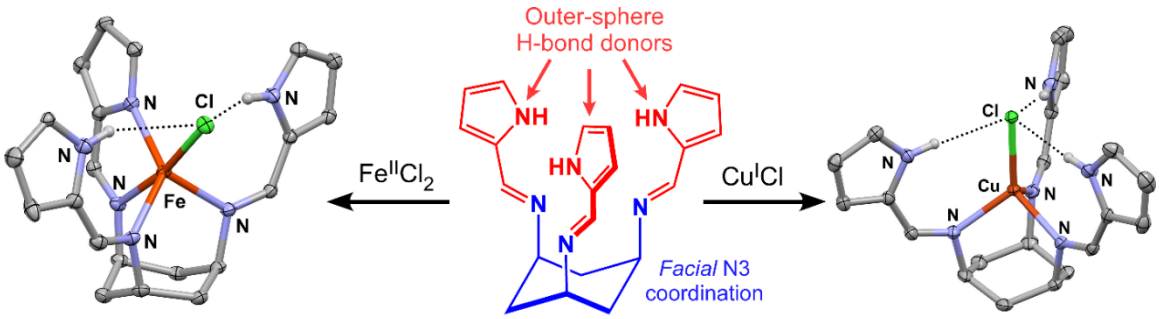

Synopsis: Ligands derived from *cis,cis*-1,3,5-triaminocyclohexane (TACH) have been prepared with pendant heterocycles that serve as outer-sphere H-bond donors. Upon coordination to Cu(I), the facially-coordinating N_3 ligands create a hydrogen-bonding cavity that stabilizes (pseudo)halide anions. Reaction of the TACH-based ligands with divalent cations revealed a range of protonation states, coordination geometries, and H-bonding interactions.